Intravital imaging of podocyte calcium in glomerular injury and disease

James L. Burford,[1] Karie Villanueva,[1] Lisa Lam,[1] Anne Riquier-Brison,[1] Matthias J. Hackl,[1,2] Jeffrey Pippin,[3] Stuart J. Shankland,[3] and János Peti-Peterdi[1]

[1]Department of Physiology and Biophysics and Department of Medicine, Zilkha Neurogenetic Institute, University of Southern California, Los Angeles, California, USA. [2]Department II of Internal Medicine and Center for Molecular Medicine Cologne, University of Cologne, Cologne, Germany. [3]Department of Medicine, Division of Nephrology, University of Washington School of Medicine, Seattle, Washington, USA.

Intracellular calcium ($[Ca^{2+}]_i$) signaling mediates physiological and pathological processes in multiple organs, including the renal podocyte; however, in vivo podocyte $[Ca^{2+}]_i$ dynamics are not fully understood. Here we developed an imaging approach that uses multiphoton microscopy (MPM) to directly visualize podocyte $[Ca^{2+}]_i$ dynamics within the intact kidneys of live mice expressing a fluorescent calcium indicator only in these cells. $[Ca^{2+}]_i$ was at a low steady-state level in control podocytes, while Ang II infusion caused a minor elevation. Experimental focal podocyte injury triggered a robust and sustained elevation of podocyte $[Ca^{2+}]_i$ around the injury site and promoted cell-to-cell propagating podocyte $[Ca^{2+}]_i$ waves along capillary loops. $[Ca^{2+}]_i$ wave propagation was ameliorated by inhibitors of purinergic $[Ca^{2+}]_i$ signaling as well as in animals lacking the P2Y2 purinergic receptor. Increased podocyte $[Ca^{2+}]_i$ resulted in contraction of the glomerular tuft and increased capillary albumin permeability. In preclinical models of renal fibrosis and glomerulosclerosis, high podocyte $[Ca^{2+}]_i$ correlated with increased cell motility. Our findings provide a visual demonstration of the in vivo importance of podocyte $[Ca^{2+}]_i$ in glomerular pathology and suggest that purinergic $[Ca^{2+}]_i$ signaling is a robust and key pathogenic mechanism in podocyte injury. This in vivo imaging approach will allow future detailed investigation of the molecular and cellular mechanisms of glomerular disease in the intact living kidney.

Introduction

Glomerular dysfunction is a common basis for the development of chronic kidney disease, a condition with significant comorbidities and mortalities. One glomerular cell type, the podocyte, plays a critical role in the maintenance of the normal structure and function of the glomerular filtration barrier (GFB), which performs plasma ultrafiltration. Podocytes are unique, highly differentiated perivascular cells around the glomerular capillaries that form interdigitating foot processes and the slit diaphragm, a key component of the GFB (1). According to the current model of podocyte pathology, rearrangement of the actin cytoskeleton is key in foot process effacement, disruption of the slit diaphragm, and albuminuria development and represents a starting point for progressive kidney disease (2). Several studies linked these pathological changes to elevated podocyte intracellular calcium ($[Ca^{2+}]_i$) (3), including the classical effects of protamine sulfate, which can cause foot process effacement in vivo (4, 5), and those of Ang II (6). Transient receptor potential channels 5 and 6 (TRPC5/6), which mediate nonselective, cationic currents in the podocyte plasma membrane, are known to regulate actin dynamics and cell motility of podocytes (7, 8), and TRPC6 gain-of-function mutations were found in families with hereditary focal segmental glomerulosclerosis (FSGS) (9, 10). The discovery that actin dynamics is regulated directly by the $[Ca^{2+}]_i$-activated phosphatase calcineurin (11), as well as the emergence of Rho GTPases as critical regulators of podocyte motility (2, 11), further support the key role of $[Ca^{2+}]_i$ signaling in podocyte function and the development of glomerular pathologies. However, our mechanistic understanding of podocyte $[Ca^{2+}]_i$ dynamics in health and disease is limited to knowledge obtained from in vitro approaches and on the above calcium channels. There may be other important and pathologically relevant mechanisms that control podocyte $[Ca^{2+}]_i$. Moreover, there are significant gaps in our understanding of how altered podocyte $[Ca^{2+}]_i$ dynamics and motility are linked to the development of albuminuria and glomerulosclerosis in the intact kidney in vivo. For example, recent data suggest a dual and context-dependent role of TRPC6 in podocytes: acute activation protects from complement-mediated damage, but chronic overactivation leads to FSGS (12). The full mechanistic understanding of podocyte $[Ca^{2+}]_i$ dynamics would be critical for the development of new therapeutic strategies targeting the podocyte in human glomerular disease.

Over the past decade, several applications of multiphoton microscopy (MPM) imaging made it possible to image the structure and function of the intact kidney in living animals with exceptional spatial and temporal resolution (13–15). The basic principles and advantages and the various past applications of this revolutionary, minimally invasive optical sectioning technique for kidney research have been reviewed recently (14). MPM imaging of mouse glomeruli in vivo is now possible (13, 16–19) and can be applied in generally available transgenic mouse models, including podocin/Cre mice (20) and a variety of fluorescent reporter mice, to establish cell-specific expression of fluorescent proteins in podocytes for imaging applications. For example, several genetically encoded calcium indicators have been developed, including the GFP-based calcium sensor GCaMP family, and their in vivo mouse models have been successfully used for neuronal imaging (21, 22).

Here we report the development of a novel imaging approach to study podocyte $[Ca^{2+}]_i$ dynamics in vivo in the intact mouse kidney, based on the combination of MPM and a new podocin/Cre-GCaMP3^{flox} mouse model (referred to herein as Pod-GCaMP3 mice). Our first applications of this new technical advance demon-

Conflict of interest: The authors have declared that no conflict of interest exists.
Citation for this article: *J Clin Invest.* 2014;124(5):2050–2058. doi:10.1172/JCI71702.

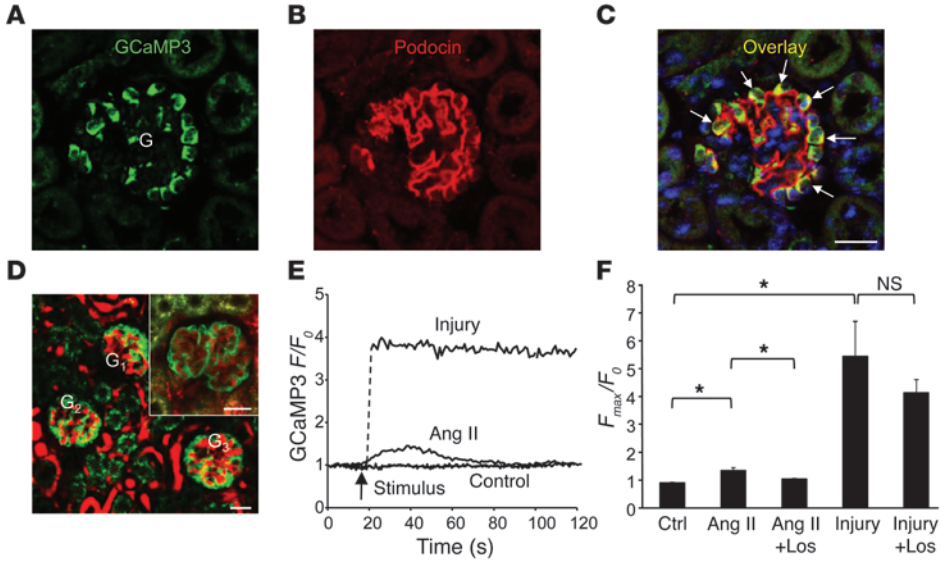

Figure 1

Characterization of the new Pod-GCaMP3 mouse model and its utility for in vivo imaging of podocyte $[Ca^{2+}]_i$. (**A**–**C**) Immunofluorescence double labeling of GCaMP3 (**A**, green) and the podocyte marker podocin (**B**, red) in a Pod-GCaMP3 mouse glomerulus (G). (**C**) The overlay image shows colocalization (yellow; arrows), confirming the podocyte-specific expression of GCaMP3 in Pod-GCaMP3 mice. Nuclei were labeled with DAPI (blue). (**D**) In vivo MPM image of the intact mouse kidney, showing the overview of podocyte-specific expression of GCaMP3 (green) in 3 adjacent glomeruli (G_1–G_3). A magnified area is shown in the inset. Scale bars: 20 μm. Plasma was labeled red with albumin–Alexa Fluor 594. Nonspecific green autofluorescence was visible in proximal tubule segments around the glomeruli. (**E**) Representative time-lapse recordings of GCaMP3 F/F_0 in single podocytes in control and during bolus Ang II injection or laser-induced podocyte injury. When the laser was used to trigger injury, GCaMP3 imaging was paused; thus, imaging for the same podocyte was noncontiguous (dashed line). (**F**) Changes in podocyte GCaMP3 F_{max}/F_0 in response to Ang II (n = 15 glomeruli from n = 5 mice) or laser-induced podocyte injury (n = 21 glomeruli from n = 9 mice), either alone or with AT_1 receptor blockade with losartan (n = 5 glomeruli per losartan group from n = 4 mice). Data represent mean ± SEM. *P < 0.05.

strated its utility in studying the role of podocyte $[Ca^{2+}]_i$ in overall glomerular function in health and disease and in exploring new control mechanisms of podocyte $[Ca^{2+}]_i$ after podocyte injury.

Results

Characterization of the Pod-GCaMP3 mouse model for in vivo imaging. We used available mouse genetic tools for the cell-specific expression of the genetically encoded calcium indicator GCaMP3 for our in vivo MPM imaging approach to study podocyte $[Ca^{2+}]_i$ in the intact kidney. Pod-GCaMP3 mice were generated by intercrossing podocin/Cre (20) and GCaMP3^{flox} reporter mice (22). Immunofluorescence colocalization of GCaMP3 and the podocyte marker podocin confirmed the podocyte-specific expression of GCaMP3 in these mice (Figure 1, A–C). Next, Pod-GCaMP3 mice were subjected to MPM imaging of the intact kidney. This new imaging approach directly visualized the structure of a number of superficial glomeruli and GCaMP3 fluorescence in podocytes in vivo with profound detail (Figure 1D). Time-lapse MPM imaging revealed low GCaMP3 fluorescence in podocytes at baseline conditions (Figure 1E and Supplemental Video 1; supplemental material available online with this article; doi:10.1172/JCI71702DS1), reflective of low $[Ca^{2+}]_i$ in healthy podocytes and its minor variations over time.

To test the ability of our imaging approach to detect alterations in podocyte $[Ca^{2+}]_i$, we first applied Ang II, which is known to trigger elevations in podocyte $[Ca^{2+}]_i$ in vitro (6). Injection of high doses of Ang II (400 ng/kg) i.v. caused minor, but significant, increases in podocyte $[Ca^{2+}]_i$, as indicated by the changes in GCaMP3 fluorescence (maximum fluorescence intensity normalized to baseline [F_{max}/F_0], 1.3 ± 0.1; n = 15 glomeruli from n = 5 mice; Figure 1, E and F). Infusion of the Ang II type 1 (AT_1) receptor blocker losartan alone did not change baseline $[Ca^{2+}]_i$ (F_{max}/F_0, 1.0 ± 0.0; n = 4 glomeruli from n = 4 mice); however, losartan pretreatment abolished the Ang II–induced elevations in podocyte $[Ca^{2+}]_i$ (F_{max}/F_0, 1.0 ± 0.0, P < 0.05; Figure 1F). We also applied a new method of focal podocyte insult by exposing a small area of a single podocyte to a short pulse of focused laser beam. In contrast to Ang II, laser-induced focal podocyte injury triggered a robust and sustained elevation in podocyte $[Ca^{2+}]_i$ around the injury site (F_{max}/F_0, 5.4 ± 1.3, P < 0.05 vs. control; n = 21 glomeruli from n = 9 mice; Figure 1, E and F). Laser injury–induced elevations in podocyte $[Ca^{2+}]_i$ were not affected significantly by losartan pretreatment (F_{max}/F_0, 4.1 ± 0.5; n = 5 glomeruli from n = 4 mice; Figure 1F).

MPM imaging of podocyte injury–induced $[Ca^{2+}]_i$ waves. In addition to the sustained elevations in podocyte $[Ca^{2+}]_i$ around the primary injury site, we observed signs of cell-to-cell propagation of high $[Ca^{2+}]_i$ to adjacent podocytes along the glomerular capillary loops, which occasionally involved the entire glomerulus. Figure 2A and Supplemental Video 2 show a representative podocyte $[Ca^{2+}]_i$ wave, based on the temporal dynamics of increased GCaMP3 fluorescence originating from the focal injury site and propagating from cell to cell to other glomerular regions. Analysis of GCaMP3 fluorescence changes in different podocytes at various distances from the primary injury site revealed the regenerating nature of the podocyte $[Ca^{2+}]_i$ wave (constant $\Delta[Ca^{2+}]_i$ regardless of distance); moreover, in most cells, the $[Ca^{2+}]_i$ response was fully reversible (Figure 2B). Importantly, the propagation of high podocyte $[Ca^{2+}]_i$ to adjacent podocytes ($[Ca^{2+}]_i$ wave) was ameliorated by i.v. infusion of the nonselective purinergic receptor antagonist suramin: F_{max}/F_0 during the $[Ca^{2+}]_i$ wave was 5.3 ± 0.9 in controls (n = 19 glomeruli from n = 9 mice) and 1.9 ± 0.2 with suramin (n = 13 glomeruli from n = 3 mice), and velocity of the $[Ca^{2+}]_i$ wave was 4.9 ± 1.0 μm/s in controls and 1.9 ± 0.5 μm/s with suramin (both P < 0.05; Figure 2C).

Quantitative MPM imaging of the effects of increased podocyte $[Ca^{2+}]_i$ on glomerular function. In addition to the direct visualization of the changes in podocyte $[Ca^{2+}]_i$ in the intact mouse kidney in vivo, this new imaging approach also allows for the study of their spatial and temporal correlations with changes in glomerular structure and function (e.g., GFB permeability to macromolecules, or capillary

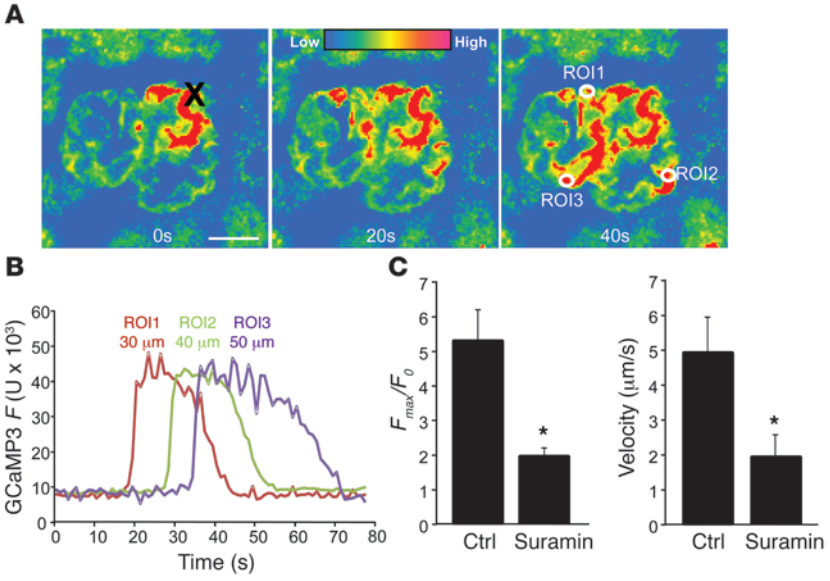

Figure 2

In vivo MPM imaging of podocyte injury–induced $[Ca^{2+}]_i$ waves propagating along the glomerular capillary loops. (**A**) The short pulse of a laser beam focused on a small focal point of a peripheral podocyte (denoted by X) caused localized, sustained high $[Ca^{2+}]_i$ around the primary injury site (red area surrounding X) and triggered a cell-to-cell $[Ca^{2+}]_i$ wave. Pseudocolor (gradient) map of GCaMP3 fluorescence intensity at the indicated time points illustrated the propagation of the podocyte $[Ca^{2+}]_i$ wave. Time-lapse MPM imaging of the same glomerulus is shown in Supplemental Video 2. Scale bar: 20 μm. (**B**) Representative recordings of GCaMP3 fluorescence in different podocytes at various distances from the primary injury site (corresponding to ROI illustrated in **A**). (**C**) Summary of podocyte $[Ca^{2+}]_i$ dynamics during wave propagation and the effects of purinergic receptor blockade with suramin. Suramin infusion (n = 13 glomeruli from n = 3 mice) significantly reduced the magnitude (F_{max}/F_0) and velocity of the $[Ca^{2+}]_i$ wave compared with control (n = 19 glomeruli from n = 9 mice). Data represent mean ± SEM. *P < 0.05 vs. control.

and glomerular diameter or area), indicative of changes in blood flow and GFR. Time-lapse MPM imaging of Pod-GCaMP3 mice in vivo during the podocyte $[Ca^{2+}]_i$ wave showed that the injury-induced increases in podocyte $[Ca^{2+}]_i$ coincided with the leakage of albumin from the plasma into the Bowman's space (Figure 3, A–C, and Supplemental Video 3). The albumin permeability of the GFB changed rather quickly: it increased essentially simultaneously with the elevation in podocyte $[Ca^{2+}]_i$ and started to decrease with reductions in podocyte $[Ca^{2+}]_i$, although complete recovery took longer for GFB albumin permeability, about 2 minutes (Figure 3C). The albumin permeability of the GFB increased almost 5-fold during the podocyte $[Ca^{2+}]_i$ wave, estimated by the increased albumin–Alexa Fluor 594 fluorescence in the Bowman's space (F_{max}/F_0, 4.8 ± 1.6; n = 16 glomeruli from n = 9 mice; Figure 3D). Importantly, suramin pretreatment prevented the albumin leakage during the podocyte $[Ca^{2+}]_i$ wave (F_{max}/F_0, 1.4 ± 0.1, P < 0.05; n = 6 glomeruli from n = 3 mice; Figure 3D). In addition, simultaneously with the increasing podocyte GCaMP3 fluorescence during the propagation of the podocyte $[Ca^{2+}]_i$ wave, a significant reduction in the size of the glomerular tuft developed within seconds (Figure 2B; Figure 3, C and E; and Supplemental Video 3), suggestive of podocyte contraction and alterations in glomerular hemodynamics. The size of the glomerular tuft area was 2,374 ± 166 μm² before the podocyte $[Ca^{2+}]_i$ wave and 2,150 ± 162 μm² at its peak (P < 0.05; n = 18 glomeruli from n = 9 mice; Figure 3E). These data provided in vivo visual confirmation of the importance of podocyte $[Ca^{2+}]_i$ in controlling key glomerular functions in conditions of podocyte injury.

Podocyte $[Ca^{2+}]_i$ imaging in vitro in microperfused glomeruli. To further study the fluorescence characteristics of GCaMP3 and the mechanistic details of the podocyte $[Ca^{2+}]_i$ wave, we used freshly dissected and in vitro–microperfused glomeruli from control and Pod-GCaMP3 mice. Using this model, we were able to reproduce the in vivo findings: mechanical stimulation (touch) of a single podocyte by a glass micropipette resulted in essentially the same cell-to-cell propagation of high $[Ca^{2+}]_i$ in podocytes (Figure 4A and Supplemental Video 4). Using preparations from GCaMP3 mice colabeled with the calcium indicator Fura Red, simultaneous monitoring of GCaMP3 and Fura Red fluorescence showed that the podocyte injury–induced $[Ca^{2+}]_i$ wave involved only podocytes, not mesangial cells or the endothelium (Figure 4B). The same podocyte injury was also applied in preparations from WT mice loaded with the calcium-sensitive fluorophore pair Fluo-4/Fura Red. Comparison of the sensitivity and accuracy of GCaMP3 versus that of Fluo-4/Fura Red to detect elevations in podocyte $[Ca^{2+}]_i$ during wave propagation revealed that the magnitude of the changes in fluorescence (i.e., changes in podocyte $[Ca^{2+}]_i$) were the same using the Fluo-4/Fura Red ratiometric (R_{max}/R_0, 2.35 ± 0.3) and the single GCaMP3 (F_{max}/F_0, 2.32 ± 0.3) fluorescence methods (n = 7 each; Figure 4C).

To further explore the role and molecular mechanism of purinergic calcium signaling in podocyte injury, genetic and pharmacological approaches were used to block the calcium wave. First, we compared podocyte $[Ca^{2+}]_i$ dynamics during wave propagation in preparations from WT mice and P2Y2 purinergic receptor KO mice using Fluo-4/Fura Red. Compared with WT control (n = 5 glomeruli), P2Y2 deficiency (n = 7 glomeruli) significantly reduced the magnitude (F_{max}/F_0; WT, 2.51 ± 0.4; P2Y2 KO, 1.18 ± 0.1, P < 0.05) and velocity (WT, 9.1 ± 3.3 μm/s; P2Y2 KO, 1.3 ± 1.2 μm/s, P < 0.05) of the $[Ca^{2+}]_i$ wave (Figure 4D). In addition, application of several chemical inhibitors to the bathing and/or perfusion solutions using control WT tissues significantly reduced the magnitude and velocity of the podocyte $[Ca^{2+}]_i$ wave (Figure 4D), including IP_3 receptor blockade with xestospongin C (XSC; F_{max}/F_0, 1.34 ± 0.2; velocity, 0.5 ± 0.5 μm/s; n = 5), gap junction (connexin) inhibition with 18 α-glycyrrhetinic acid (18α-GA; F_{max}/F_0, 1.28 ± 0.2; velocity, 0.8 ± 0.8 μm/s; n = 4), and extracellular ATP scavenging with a cocktail of apyrase combined with hexokinase (F_{max}/F_0, 1.12 ± 0.1, velocity: 1.4 ± 1.0 μm/s; n = 4).

Podocyte $[Ca^{2+}]_i$ imaging in vivo in disease models. We applied this new imaging approach in 2 clinically relevant disease models to show the feasibility of directly visualizing the changes and role of podocyte $[Ca^{2+}]_i$ in vivo in renal pathology. Renal fibrosis (unilateral ureteral obstruction [UUO]) or experimental glomerular disease (FSGS model, characterized by abrupt podocyte depletion)

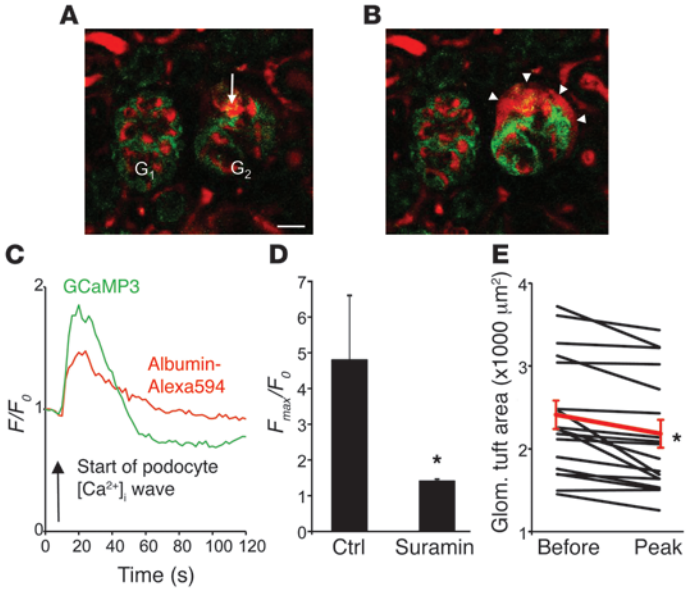

Figure 3
Quantitative MPM imaging of the effects of increased podocyte $[Ca^{2+}]_i$ on glomerular function in vivo. (**A** and **B**) Representative MPM images of an intact (G_1) and an adjacent laser-injured glomerulus (G_2; arrow denotes injury site) from an intact Pod-GCaMP3 mouse kidney before (**A**) and during (**B**) the podocyte $[Ca^{2+}]_i$ wave. In **B**, increased GCaMP3 fluorescence (green) indicates increased podocyte $[Ca^{2+}]_i$, whereas increased red fluorescence in the Bowman's space (arrowheads) indicates concomitant leakage of plasma albumin–Alexa Fluor 594 in the injured glomerulus, but not the adjacent intact glomerulus. Scale bar: 20 μm. (**C**) Dynamics of the elevations in GCaMP3 (measured in the glomerular tuft) and albumin–Alexa Fluor 594 (measured in the Bowman's space) F/F_0 during the podocyte $[Ca^{2+}]_i$ wave in the same preparation as in **A** and **B**. (**D**) Albumin leakage into the Bowman's space during podocyte $[Ca^{2+}]_i$ wave propagation and the effects of purinergic receptor blockade with suramin. Suramin infusion ($n = 6$ glomeruli from $n = 3$ mice) significantly reduced the magnitude of the peak increase in Bowman's space albumin–Alexa Fluor 594 F_{max}/F_0 compared with control ($n = 16$ glomeruli from $n = 9$ mice). Data represent mean ± SEM. (**E**) Size of the glomerular tuft area before and at the peak of the podocyte $[Ca^{2+}]_i$ wave ($n = 18$ glomeruli from $n = 9$ mice each). Mean ± SEM is shown in red. *$P < 0.05$ vs. respective control.

was induced in Pod-GCaMP3 or Pod-GFP mice, and fluorescence intensity in podocytes was followed during the initial phases of glomerular pathology. MPM imaging demonstrated that compared with stationary podocytes, which had low steady-state GCaMP3 fluorescence intensity (i.e., low $[Ca^{2+}]_i$), podocytes that appeared to cluster or migrate to the parietal layer of the Bowman's capsule showed high GCaMP3 fluorescence (i.e., high $[Ca^{2+}]_i$; Figure 5, A and D). GCaMP3 fluorescence in motile podocytes increased >10-fold in the UUO model over time (day 10 after UUO, 906 ± 142 AU; day 12, 2,746 ± 399 AU, $P < 0.05$ vs. day 10; day 16, 11,232 ± 1,422 AU, $P < 0.05$ vs. day 12; $n = 5$–15 glomeruli each; Figure 5C). Due to the rapidly developing pathology in the cytotoxic IgG–induced FSGS model (23, 24), the present studies examined only the early changes through the first 4 days after induction. GCaMP3 fluorescence in clustering podocytes increased >2-fold over time (day 3 after induction, 3,811 ± 395 AU; day 4, 8,387 ± 332 AU, $P < 0.05$; $n = 9$–15 glomeruli each; Figure 5F). To ascertain that increased GCaMP3 fluorescence reflected increased podocyte $[Ca^{2+}]_i$ and not increased protein expression, the same disease models were applied in Pod-GFP mice as control. GFP expression in these mice is an appropriate control for protein expression, since the Cre that activated GCaMP3 and GFP was expressed under the same promoter (podocin) in Pod-GCaMP3 and Pod-GFP mice, respectively. Moreover, both fluorescent reporters were in the same ROSA26 locus. During the same period, no significant changes or even reduction were observed in podocyte GFP fluorescence, although podocyte clustering and migration were still present (Figure 5, B, C, E, and F).

Discussion

In this study, we developed a new imaging approach to directly visualize $[Ca^{2+}]_i$ dynamics in the critically important but inaccessible renal cell type of podocytes in vivo in the intact kidney. The applied method was the combination of intravital MPM with transgenic mice that stably express the improved genetically encoded fluorescent indicator GCaMP3 selectively in podocytes, under the control of the podocin promoter. Our findings indicated that MPM imaging of Pod-GCaMP3 transgenic mice represents an excellent tool for detecting changes in podocyte $[Ca^{2+}]_i$ and associated alterations in glomerular function in vivo in health and disease. Therefore, this new approach solves a critical technical barrier in kidney research and allows for detailed investigation of the molecular and cellular mechanisms of albuminuria and glomerulosclerosis in the intact living kidney. We demonstrated the utility of this new technical advance in several pioneering applications. First, we showed that the baseline and agonist-induced dynamic changes in podocyte $[Ca^{2+}]_i$ could be detected in the intact glomerular environment in a minimally invasive manner with high spatial and temporal resolution. Second, a new podocyte injury model was applied, which revealed cell-to-cell propagation of a podocyte $[Ca^{2+}]_i$ wave as a newly discovered feature of primary and secondary podocyte injury. Third, large and robust $[Ca^{2+}]_i$ signals were detected in response to podocyte injury, likely the result of purinergic $[Ca^{2+}]_i$ signaling, a newly established key $[Ca^{2+}]_i$ pathway in podocyte pathology. Fourth, in vivo MPM imaging of podocyte $[Ca^{2+}]_i$ was performed together with quantitative imaging of glomerular functional parameters for the complex visual analysis of renal and glomerular pathology. Finally, this is the first time that changes in $[Ca^{2+}]_i$ were followed in any disease state in vivo. Our results were suggestive of a correlation between increased podocyte $[Ca^{2+}]_i$ and cell motility in 2 highly clinically relevant disease models of kidney fibrosis (UUO) and FSGS (cytotoxic IgG), and highlighted how podocyte $[Ca^{2+}]_i$ dynamics intertwine with the progression of glomerular diseases. Together, these results indicate that this newly established imaging approach will be useful in future work studying the role and molecular mechanisms of podocyte $[Ca^{2+}]_i$ dynamics in glomerular disease.

Until recently, fluorescence imaging with traditionally used, synthetic Ca^{2+}-sensitive dyes has been the method of choice by which to study $[Ca^{2+}]_i$-dependent functions of several cell types, including in the kidney. In the present study, however, we used the genetically encoded fluorescent indicator GCaMP3 to achieve cell-specific delivery and to avoid the many technical difficulties associated with in vivo delivery and use of classical acetoxymethylester-based (AM-based) fluorophores (14). In Pod-GCaMP3 mice, GCaMP3 was expressed selectively in podocytes with diffuse cytosolic distribution and showed a

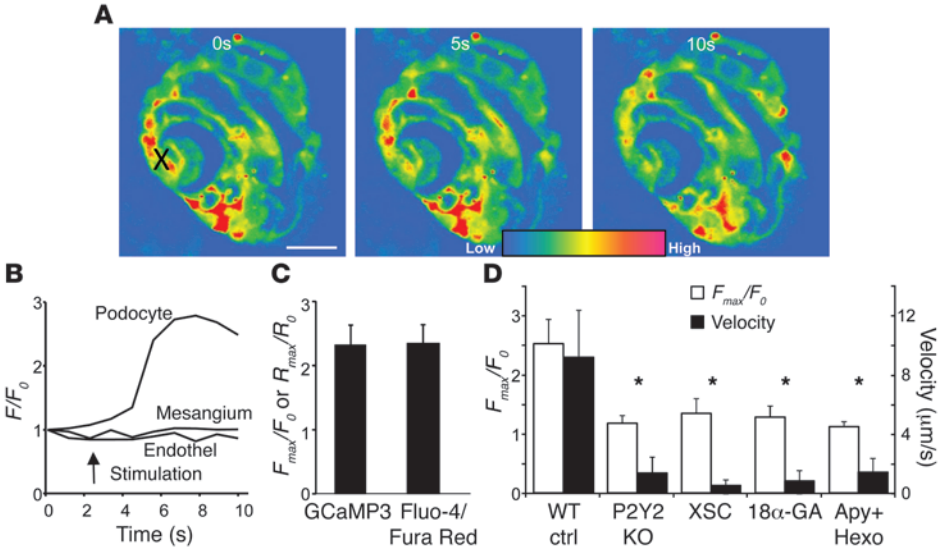

Figure 4

Podocyte $[Ca^{2+}]_i$ imaging in vitro in microperfused glomeruli. (**A**) Pseudocolor (gradient map) of GCaMP3 fluorescence intensity from Pod-GCaMP3 mice showed the highly elevated $[Ca^{2+}]_i$ in WT podocytes around the site of acute injury, caused mechanically by touching a single podocyte with a glass micropipette (denoted by X). The high $[Ca^{2+}]_i$ propagated to adjacent podocyte regions ($[Ca^{2+}]_i$ wave) along capillary loops within 10 seconds. Time-lapse imaging of the same glomerulus is shown in Supplemental Video 4. Scale bar: 20 μm. (**B**) Acute podocyte injury (arrow) induced robust elevation in $[Ca^{2+}]_i$ in podocytes, measured by GCaMP3 F/F_0, but not in mesangial and endothelial cells (identified based on anatomical features), as measured by Fura Red F/F_0, which was used in the same preparation. (**C**) Magnitude of injury-induced podocyte $[Ca^{2+}]_i$ elevations, measured by single GCaMP3 fluorescence (F_{max}/F_0) or Fluo-4/Fura Red ratiometric (R_{max}/R_0) methods ($n = 7$ each). (**D**) Genetic and pharmacological blockade of the podocyte $[Ca^{2+}]_i$ wave. P2Y2 deficiency ($n = 7$ glomeruli), IP_3 receptor blockade with XSC ($n = 5$), gap junction inhibition with 18α-GA ($n = 4$), and ATP scavenging with the cocktail of apyrase plus hexokinase ($n = 4$) all significantly reduced the magnitude (F_{max}/F_0) and velocity of the $[Ca^{2+}]_i$ wave compared with WT controls ($n = 5$). Data represent mean ± SEM. *$P < 0.05$ vs. WT.

low level of fluorescence in control mice (Figure 1, A–D). Like other Ca^{2+} fluorophores, GCaMP3 may buffer Ca^{2+} and therefore interfere with cell signaling. However, we observed no signs of altered subcellular localization (e.g., nuclear) that would indicate this (21), and Pod-GCaMP3 mice showed no gross morphological or functional abnormalities (e.g., proteinuria) compared with WT mice (data not shown). These results indicated that Pod-GCaMP3 mice exhibit stable, long-term expression of GCaMP3 in podocytes with normal functions and thus allow for the sensitive detection of podocyte $[Ca^{2+}]_i$ dynamics in vivo using MPM.

MPM is a powerful, minimally invasive imaging technique for the deep optical sectioning of living tissues. The basic principles, applications, advantages, and limitations of this imaging technology for the study of the living intact kidney, including the GFB, have been recently described in detail (14). The first applications of MPM on the intact living kidney (15) were subsequently improved to directly and quantitatively visualize the permeability of the GFB to albumin and other macromolecules (25, 26) as well as podocyte motility/migration in health and disease in vivo (16, 19). The feasibility of routinely performing MPM imaging of glomeruli in the intact kidney of several mouse strains has been confirmed by several laboratories (13, 14, 17, 18).

The first applications of this new imaging approach indicated that time-lapse MPM imaging of Pod-GCaMP3 mouse kidneys represents a useful tool with which to directly visualize, in vivo and over time (i.e., during disease progression), the dynamics of podocyte $[Ca^{2+}]_i$ and the associated structural and functional changes in the intact glomerulus with high resolution. Our results provided important in vivo visual confirmation of previously reported in vitro changes in podocyte $[Ca^{2+}]_i$ and demonstrated the critical importance and role of podocyte $[Ca^{2+}]_i$ in controlling key glomerular functions. The low podocyte $[Ca^{2+}]_i$ levels found at baseline in control mice confirmed previous reports that healthy podocytes appear to work hard to maintain the lowest $[Ca^{2+}]_i$ among all cell types in the glomerulus (27), which may be the result of efficient Ca^{2+} extrusion (28) and various cell-specific $[Ca^{2+}]_i$ sinks (3, 29). These mechanisms are thought to maintain low global $[Ca^{2+}]_i$ in order to allow dynamic and compartmentalized $[Ca^{2+}]_i$ changes and their delicate control of the actin cytoskeleton (3). Our new approach was also able to visualize high podocyte $[Ca^{2+}]_i$ in response to various stress stimuli and its pathogenic role in causing glomerular dysfunction. Ang II, a well-established pathogenic mechanism in glomerular injury, is known to cause elevated podocyte $[Ca^{2+}]_i$ in vitro (6), an effect that involves TRPC5/6 nonselective cation channels (3, 30) and is implicated in glomerulosclerosis (9). Ang II caused small but significant elevations in podocyte $[Ca^{2+}]_i$ in vivo that were inhibited by the AT_1 receptor blocker losartan (Figure 1, E and F), consistent with earlier studies on the role of Ang II and AT_1 receptor in these cells (6). However, the Ang II–induced changes in $[Ca^{2+}]_i$ were minor compared with the robust effects of direct podocyte injury, which were not inhibited by losartan, and therefore did not involve endogenous Ang II or the AT_1 receptor (Figure 1, E and F, and Figure 2C). However, an interaction between Ang II and P2 purinergic receptor signaling in injury models and disease conditions is possible, and will require further study.

In terms of the podocyte injury model, a short pulse of laser beam was used to induce well-controlled, localized, reproducible, acute, and titratable (based on laser power and size of region of interest [ROI] scan area) podocyte injury that can be applied anywhere in the glomerulus. The laser-induced cell injury was focal, transient, and reversible in nature, likely caused by local heat induction resulting in temporarily increased cell membrane permeability. We never observed leakage of GCaMP3 from within the cell, podocyte loss (cell death), or exit via urinary space, which require much higher laser exposure to develop, as we previously demonstrated (16). This technique was recently described and tested by our laboratory (14, 16). Importantly, laser or mechanically induced podocyte injury appeared to be mediated, at least in part, by P2

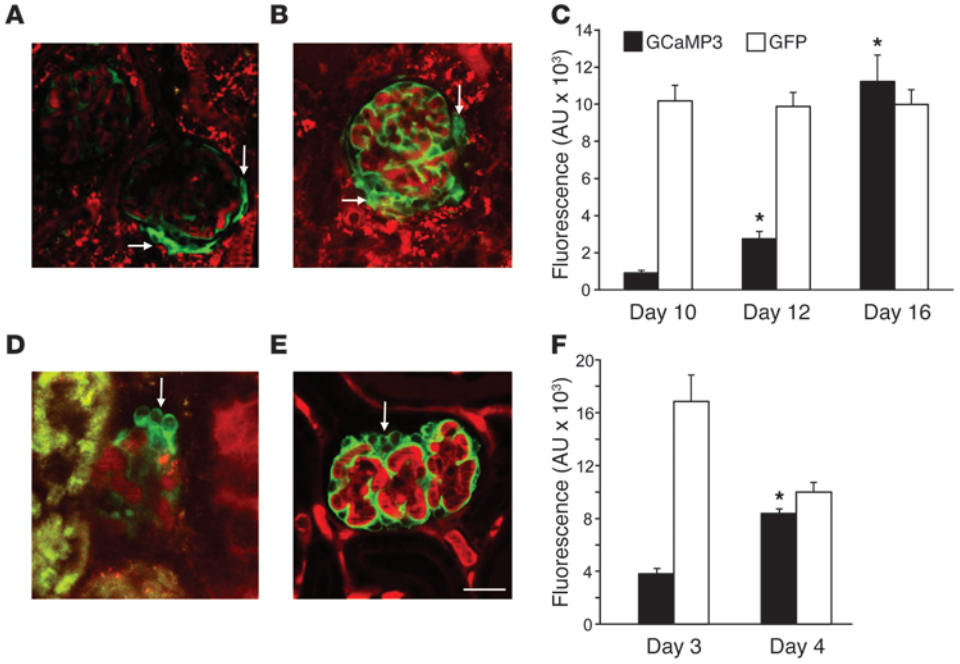

Figure 5
In vivo MPM imaging of glomerular disease–induced changes in podocyte $[Ca^{2+}]_i$. Changes in fluorescence were assessed 3–16 days after unilateral ureter obstruction (UUO; **A**–**C**; *n* = 5–15 glomeruli) or induction of glomerular disease resembling classic clinical FSGS (**D**–**F**; *n* = 9–15 glomeruli). (**A**–**D**) Podocyte GCaMP3 (**A** and **D**) and GFP (**B** and **E**) fluorescence (green) in Pod-GCaMP3 and Pod-GFP mice, respectively. Intravascular space (plasma) was labeled red with i.v. injected albumin–Alexa Fluor 594. Arrows denote podocytes clustering or migrating to the parietal layer of Bowman's capsule. Scale bar: 20 μm. (**C** and **F**) Dynamics of podocyte GCaMP3 ($[Ca^{2+}]_i$) or GFP fluorescence intensity changes 10–16 days after UUO (**C**) or 3–4 days after FSGS induction (**F**). Data represent mean ± SEM. *$P < 0.05$ vs. the earlier time point.

purinoceptors, including P2Y2 (Figure 2C and Figure 4D). These results suggest a new and important role of P2 receptor–mediated purinergic Ca^{2+} signaling in glomerular pathology and present the P2Y2 receptor as a potential new therapeutic target. The robust in vitro effects of extracellular ATP on podocyte $[Ca^{2+}]_i$ (31) and the expression of the P2Y2 purinergic receptor exclusively in podocytes in the native and isolated rat glomerulus (32) have been reported previously. Due to the expression of other P2 receptor subtypes in podocytes (e.g., P2Y1), at least in the rat kidney (33), further studies are needed to determine the role and molecular players of podocyte purinergic $[Ca^{2+}]_i$ signaling in glomerular pathologies.

In addition to visualizing podocyte $[Ca^{2+}]_i$ in vivo for the first time during glomerular injury and disease progression, this new imaging approach allows simultaneous quantitative functional analysis of the glomerulus. This includes the measurement of albumin permeability of the intact GFB and glomerular tuft contraction (Figure 3, A–E), which reflect changes in glomerular filtration rate. Other basic parameters of glomerular and kidney function may also be measured with MPM imaging, as established recently (13, 25, 26). The temporary albumin leakage and podocyte/glomerular tuft contraction that were quantitatively visualized during progressive increases in podocyte $[Ca^{2+}]_i$ in vivo for the first time (Figure 3, A–D) demonstrated the rapid (within a few seconds), highly dynamic, and reversible nature of these phenomena in the intact glomerular environment. The leakage of albumin usually appeared first around the injury site (coinciding with high $[Ca^{2+}]_i$) and then gradually developed around nearby capillary segments, simultaneously with the propagation of the $[Ca^{2+}]_i$ wave to those segments. Depending on the location of the primary injury (urinary versus vascular pole, or in between), and the intensity and direction of the $[Ca^{2+}]_i$ wave on the particular confocal section, in some images the leakage was more apparent in certain regions of the Bowman's space, but usually involved the entire glomerulus (Figure 3, A and B, and Supplemental Video 3). Importantly, suramin pretreatment prevented the albumin leakage in this model of focal podocyte injury (Figure 3D), which suggests that the propagation of the high $[Ca^{2+}]_i$ signal (wave) was important for the focal disruption of the glomerular barrier. These results are consistent with the established roles of podocyte $[Ca^{2+}]_i$ in cell motility and of actin cytoskeleton and slit diaphragm remodeling (foot process effacement) in glomerular disease and albuminuria development (3). Recent advances in the optical imaging of podocyte foot processes (34) in the living glomerulus (35) may permit simultaneous visualization of the changes in podocyte $[Ca^{2+}]_i$ and cell ultrastructure and the alterations in local GFB albumin permeability in Pod-GCaMP3 mice in future studies.

Cell-to-cell propagation of the high podocyte $[Ca^{2+}]_i$ (calcium wave) mediated by extracellular ATP and purinergic signaling may be a new mechanism in secondary podocyte injury, consistent with the concept that podocyte injury damages other podocytes (the amplified cascade of podocyte injury) (36). Although the expression of connexin 43 in podocytes has been reported, suggestive of gap junctional intercellular communication between podocytes (37), our results were only partially consistent with this possibility. The nonspecific gap junction uncoupler 18α-GA significantly inhibited the podocyte $[Ca^{2+}]_i$ wave (Figure 4D); however, 18α-GA also blocks mechanosensitive, ATP-releasing connexin hemichannels that are involved in cell-to-cell purinergic $[Ca^{2+}]_i$ signaling (38). Moreover, the diffusion of second messengers Ca^{2+} or IP_3 through gap junctions is a known mechanism to link $[Ca^{2+}]_i$ responses of adjacent cells (39). Our finding that the IP_3 receptor antagonist XSC inhibited the podocyte $[Ca^{2+}]_i$ wave (Figure 4D) may be consistent with gap junctional communication in podocytes; however, IP_3 receptor–mediated Ca^{2+} mobilization can also be involved in P2 purinoceptor signaling. Most importantly, the podocyte $[Ca^{2+}]_i$ wave was completely inhibited by scavenging extracellular ATP (Figure 4D), which further supports the primary role of purinergic rather than gap junctional intercellular communication between podocytes. The relatively low speed of the $[Ca^{2+}]_i$ wave propagation (Figure 4D) and the sustained, isolated high $[Ca^{2+}]_i$ in podocyte clusters in injury models (Figure 5) also argue against gap junctional communication. It should be also

noted that in most preparations, the same, reproducible podocyte $[Ca^{2+}]_i$ waves were observed, regardless of the location of primary podocyte injury. Injury of podocytes at the urinary versus vascular pole of the glomerulus produced similar results (data not shown), which suggests that active cell-to-cell propagation (ATP release, purinergic $[Ca^{2+}]_i$ signaling, $[Ca^{2+}]_i$-induced ATP release, and so on) was the underlying mechanism, rather than extracellular diffusion of the mediator substance (ATP). The regenerating nature of the podocyte $[Ca^{2+}]_i$ wave (Figure 2B) further supports active propagation versus mediator diffusion. Similar propagation of purinergic $[Ca^{2+}]_i$ waves were found in several cell types, including the cells of the in vitro–microperfused glomerulus (27) and the glomerular endothelium (38).

The single GCaMP3 fluorescence method presented here provided highly sensitive and accurate measurement of the relative changes in podocyte $[Ca^{2+}]_i$, both in vivo and in vitro during various experimental maneuvers. This was confirmed by the identical relative changes in podocyte $[Ca^{2+}]_i$ detected by the single GCaMP3 and classical Fluo-4/Fura Red ratiometric approaches (Figure 4C). Similarly to its previous applications in other cell types and organs (21, 22), the robust, several-fold increases in GCaMP3 fluorescence allows single-channel detection of $[Ca^{2+}]_i$ without the need for ratiometric measurements. Even more sensitive versions of GCaMPs were developed recently (e.g., GCaMP5 and GCaMP6; refs. 40, 41), which may be used for several future intravital applications.

Use of this new imaging approach in vivo in renal disease models, such as those shown in Figure 5, should help to better understand the mechanistic details and the role of podocyte $[Ca^{2+}]_i$ in the development of renal pathologies. At least in the presently applied disease models of kidney fibrosis (UUO) and FSGS (cytotoxic IgG), a slow, steady rise was observed in podocytes, rather than rapid and sustained high $[Ca^{2+}]_i$ (Figure 5), consistent with the slowly progressive nature of these diseases. In addition, the heterogeneous distribution of podocyte clusters with high $[Ca^{2+}]_i$ along select glomerular capillaries after cytotoxic IgG treatment (Figure 5D) resembled the typical focal segmental pattern of FSGS pathology. Also, consistent with our recent report that podocytes can migrate to the parietal Bowman's capsule after UUO (19), our present studies found high $[Ca^{2+}]_i$ in those podocytes that made contact with the parietal layer or apparently migrated to the parietal Bowman's capsule (Figure 5A). These results provide important insights into changes in podocyte $[Ca^{2+}]_i$ during disease progression and directly show the association of high podocyte $[Ca^{2+}]_i$ with podocyte clustering and migration in UUO and FSGS (Figure 5). Our data are consistent with earlier reports on the role of $[Ca^{2+}]_i$ in podocyte motility (3, 7, 9–11). It should be noted, however, that the present finding of high $[Ca^{2+}]_i$ in motile or migrating podocytes is merely a correlation. To determine whether high podocyte $[Ca^{2+}]_i$ plays a direct causative role in cell migration, and other pathogenic (9) or protective (12) roles in various glomerular diseases, and to clarify which podocyte $[Ca^{2+}]_i$ regulating molecular mechanisms are most significant, will require further study.

In summary, the present studies describe the development and first applications of a new imaging approach to visualize podocyte $[Ca^{2+}]_i$ in vivo in the intact glomerular environment and in glomerular disease states, which is an important technical breakthrough in kidney disease research. Our results suggest that purinergic $[Ca^{2+}]_i$ signaling is a robust and key novel pathogenic mechanism in podocyte injury. MPM imaging of Pod-GCaMP3 mice allows for complex and dynamic investigation of Ca^{2+}-coupled key podocyte signaling mechanisms and their associated effects on glomerular (dys)function in the intact living kidney. Future use of this new imaging approach may provide important insights into glomerular disease processes and may help to identify novel therapeutic targets for the treatment of kidney diseases.

Methods

Animals. C57BL6/J mice 3–6 weeks of age were used. Pod-GCaMP3 fluorescent reporter mice, which specifically express the intensely green and calcium-sensitive fluorescent protein GCaMP3 in podocytes, were generated by crossing mice expressing Cre recombinase under the control of the podocin promoter (20) and GCaMP3^{flox} mice (22). Both of these mice and P2Y2 purinergic receptor KO mice were purchased from the Jackson laboratory. Generation and use of Pod-GFP mice was described recently (19).

MPM imaging. Animals were anesthetized with a combination of ketamine (100 mg/kg) and xylazine (10 mg/kg). A trachea tube was placed to facilitate breathing, and the right carotid artery and/or jugular vein was cannulated for dye infusion. Alexa Fluor 594–conjugated bovine serum albumin was injected i.v. to label the vasculature. The left kidney was exteriorized through a flank incision, and the animal was placed on the microscope stage as described previously (13). Body temperature was maintained with a homeothermic blanket system (Harvard Apparatus). Optical sectioning of the intact kidney in vivo was performed using a Leica TCS SP5 multiphoton confocal fluorescence imaging system (Leica Microsystems) with a ×63 Leica glycerine-immersion objective (NA 1.3) powered by a Chameleon Ultra-II MP laser at 860–920 nm (Coherent) and a DMI 6000 inverted microscope's external nondescanned detectors with TRITC (red channel) and FITC (green channel) filters.

Podocyte injury. Acute podocyte injury was induced by focusing the laser beam on a small focal point at the periphery of a GCaMP3-positive cell (approximately 1-μm × 1-μm square-shaped ROI scan for 1 second at 20% laser power) to induce well-controlled and localized injury of a single podocyte. This technique was recently described by our laboratory for the injury of endothelial cells within glomerular capillaries (16) and for injuring the entire GFB (14).

UUO disease model. UUO is an animal model widely used to study progressive renal disease and tubulointerstitial fibrosis (42, 43). Between 3 and 8 weeks of age, animals were anesthetized with isoflurane, and after a midline laparotomy, the left ureter was exposed and ligated 3 times. Successful ligation was confirmed by the hydronephrotic distension of the kidney at the time of imaging.

Experimental FSGS disease model. An inducible model of experimental glomerular disease resembling classic clinical FSGS was induced with a cytotoxic antibody. Generation and characterization of these sheep anti-rabbit glomerular antibodies, which bind selectively to podocytes, have been described previously (23, 24). This experimental FSGS model induces an abrupt decline in podocyte number, which is associated clinically with proteinuria onset and histologically with FSGS (23, 24). Disease was induced by administering 12.5 mg/20 g BW sheep anti-rabbit glomerular IgG antibodies in a single i.p. injection.

Time-lapse calcium imaging. An optical section in the midportion of a superficial glomerulus was selected, and time (xyt) series with 1 frame per second were recorded before and after podocyte injury. The strong, positive, cell-specific signal (GCaMP3 fluorescence) and high-resolution MPM imaging allowed for easy identification of single podocyte cell bodies (without processes). ROI were drawn closely over the total cell body of single podocytes on confocal images (Figure 2A), around and at different distances from the damage site, and the changes in mean GCaMP3 F/F_0 (green channel; fluorescence intensity expressed as a ratio relative to baseline) were measured after the experiment in the defined

ROI using the Quantify package of LAS AF Lite software (2.0.2 build 2038; Leica-Microsystems). In the applied disease models, when the positive cells were not uniformly distributed (see Figure 5), GCaMP3 and GFP F/F_0 were measured in ROI that were hand-drawn closely over the total cell body of multicell podocyte clusters located either at the visceral or parietal Bowman's capsule. The increased albumin permeability of the GFB was assessed by the change in albumin–Alexa Fluor 594 F/F_0 in the Bowman's space (red channel; fluorescence intensity expressed as a ratio normalized to baseline) (25). The changes in glomerular tuft area were measured using Leica LAS AF software quantification tools. In some mice, Ang II (400 ng/kg BW; Phoenix Phamaceuticals), the purinergic receptor inhibitor suramin (50 mg/kg bolus, followed by 150 mg/kg/h maintenance infusion; Sigma-Aldrich) (44) and/or the AT_1 receptor blocker losartan (9.9 mg/kg BW; Sigma-Aldrich) (45) were administered by i.v. infusion. The efficient dosing and intrarenal delivery of Ang II was confirmed by its robust effects of glomerular hemodynamics, e.g., efferent arteriole contraction (data not shown).

Freshly dissected and in vitro microperfused glomerulus. Individual glomeruli with attached afferent arteriole (AA) were dissected freehand from freshly harvested kidneys of anesthetized WT or Pod-GCaMP3 mice and perfused in vitro using methods that were described previously (27). Briefly, the AA was cannulated and microperfused, and the entire preparation was loaded with Fluo-4/Fura Red–AM added to the perfusate (1 μM; Invitrogen) at 25°C for 15 minutes for single GCaMP3 or Fluo-4/Fura Red ratiometric $[Ca^{2+}]_i$ imaging. Dissection media were prepared from DMEM mixture F12 (Sigma-Aldrich). Fetal bovine serum (Hyclone) was added at a final concentration of 3%. Arteriole perfusion and bath fluid was a modified Krebs-Ringer–HCO_3 buffer containing 110 mM NaCl, 25 mM $NaHCO_3$, 0.96 mM NaH_2PO_4, 0.24 mM Na_2HPO_4, 5 mM KCl, 1.2 mM $MgSO_4$, 2 mM $CaCl_2$, 5.5 mM D-glucose, and 100 μM L-arginine. Each preparation was transferred to a thermoregulated Lucite chamber mounted on an inverted microscope (Leica IRE2; ×63 1.3NA oil immersion objective). The preparation was kept in the dissection solution; temperature was kept at 4°C until cannulation of the arteriole was completed, then gradually increased to 37°C for the remainder of the experiment. The bath was continuously exchanged (1 ml/min) and oxygenized (95% O_2, 5% CO_2) throughout the experiment. In this preparation, a single podocyte was selected for direct mechanical stimulation (touch) of the cell's surface with the tip of a perfusion pipette (2–3 μm diameter) (46). Elevations in podocyte $[Ca^{2+}]_i$ were monitored by increases in GCaMP3 F/F_0 or in Fluo-4/Fura Red R/R_0. In some preparations from GCaMP3 mice, Fura Red was loaded for simultaneous measurement of mesangial and endothelial $[Ca^{2+}]_i$. Mesangial cells (inside the glomerular tuft between perfused capillary loops and in continuum with the typical extraglomerular mesangium) and endothelial cells (bulging cell bodies inside the lumen of perfused glomerular capillaries) were identified based on anatomical considerations (Supplemental Video 4). Fluorescence emission was detected every 2 seconds at 530 ± 20 nm (for GCaMP3 and Fluo-4) or >600 nm (for Fura Red) in response to excitation at 488 nm using a Leica TCS SP2 AOBS MP confocal microscope system, as described previously (27). Fluorescence intensity measurements were performed in ROI drawn closely over the total cell body of single cells on confocal images using the Quantify package of LAS AF Lite software (2.0.2 build 2038, Leica-Microsystems). In some experiments, the IP_3 receptor blocker XSC (20 μmol/l; Sigma-Aldrich), the gap junction (connexin) inhibitor 18α-GA (25 μmol/l; Sigma-Aldrich), or the extracellular ATP scavenging cocktail of apyrase plus hexokinase (50 U/ml each; Sigma-Aldrich) was applied to the bathing and/or perfusion solutions.

Immunohistochemistry. Animals were anesthetized and perfused with ice-cold PBS into the left ventricle followed by ice-cold 4% PFA for 2 minutes each, and harvested kidney slices were embedded in OCT. Frozen kidney sections (6 μm) were postfixed in 4% PFA and incubated with goat anti-podocin primary (1:100; Sigma-Aldrich) and donkey anti-goat Alexa Fluor 594–conjugated secondary (1:500; Invitrogen) antibodies for 1 hour each at room temperature. Subsequent immunofluorescence labeling was performed to enhance GCaMP3 fluorescence by overnight incubation at 4°C with 1:1,000 dilution of rabbit anti-GFP (Invitrogen) primary antibodies (which recognize GCaMP3) followed by 4 hours of incubation at room temperature with goat anti-rabbit secondary antibodies (1:500; Invitrogen) conjugated with Alexa Fluor 488. Confocal fluorescence microscopy was performed using the same Leica TCS SP5 microscope as described above.

Statistics. Data are expressed as mean ± SEM and were analyzed using 2-tailed Student's *t* test. A *P* value less than 0.05 was considered significant.

Study approval. All animal protocols were approved by the IACUC at the University of Southern California.

Acknowledgments

This work was supported in part by NIH grants R01DK64324 (to J. Peti-Peterdi) and R01DK056799 and R21DK081835 (to S.J. Shankland). M.J. Hackl was supported by Deutsche Forschungsgemeinschaft grant HA-6212. A. Riquier-Brison is funded by a postdoctoral research fellowship of the American Heart Association. The authors thank Han Wang (University of Southern California) for thoughtful discussions on GCaMP3 models.

Received for publication December 16, 2013, and accepted in revised form February 20, 2014.

Address correspondence to: János Peti-Peterdi, Department of Physiology and Biophysics and Department of Medicine, Zilkha Neurogenetic Institute, University of Southern California, 1501 San Pablo Street, ZNI 335, Los Angeles, California 90033, USA. Phone: 323.442.4337; Fax: 323.442.4466; E-mail: petipete@usc.edu.

1. Pavenstadt H, Kriz W, Kretzler M. Cell biology of the glomerular podocyte. *Physiol Rev*. 2003; 83(1):253–307.
2. Faul C, Asanuma K, Yanagida-Asanuma E, Kim K, Mundel P. Actin up: regulation of podocyte structure and function by components of the actin cytoskeleton. *Trends Cell Biol*. 2007;17(9):428–437.
3. Greka A, Mundel P. Balancing calcium signals through TRPC5 and TRPC6 in podocytes. *J Am Soc Nephrol*. 2011;22(11):1969–1980.
4. Seiler M, Venkatachalam M, Cotran R. Glomerular epithelium: structural alterations induced by polycations. *Science*. 1975;189(4200):390–393.
5. Rudiger F, Greger R, Nitschke R, Henger A, Mundel P, Pavenstadt H. Polycations induce calcium signaling in glomerular podocytes. *Kidney Int*. 1999; 56(5):1700–1709.
6. Henger A, et al. Angiotensin II increases the cytosolic calcium activity in rat podocytes in culture. *Kidney Int*. 1997;52(3):687–693.
7. Tian D, et al. Antagonistic regulation of actin dynamics and cell motility by TRPC5 and TRPC6 channels. *Sci Signal*. 2010;3(145):ra77.
8. Schaldecker T, et al. Inhibition of the TRPC5 ion channel protects the kidney filter. *J Clin Invest*. 2013; 123(12):5298–5309.
9. Winn MP, et al. A mutation in the TRPC6 cation channel causes familial focal segmental glomerulosclerosis. *Science*. 2005;308(5729):1801–1804.
10. Reiser J, et al. TRPC6 is a glomerular slit diaphragm-associated channel required for normal renal function. *Nat Genet*. 2005;37(7):739–744.
11. Faul C, et al. The actin cytoskeleton of kidney podocytes is a direct target of the antiproteinuric effect of cyclosporine A. *Nat Med*. 2008;14(9):931–938.
12. Kistler AD, et al. TRPC6 protects podocytes during complement-mediated glomerular disease. *J Biol Chem*. 2013;288(51):36598–36609.
13. Kang JJ, Toma I, Sipos A, McCulloch F, Peti-Peterdi J. Quantitative imaging of basic functions in renal (patho)physiology. *Am J Physiol Renal Physiol*. 2006; 291(2):F495–F502.
14. Peti-Peterdi J, Burford JL, Hackl MJ. The first decade of using multiphoton microscopy for high-power kidney imaging. *Am J Physiol Renal Physiol*. 2012; 302(2):F227–F233.
15. Dunn KW, et al. Functional studies of the kidney of living animals using multicolor two-photon microscopy. *Am J Physiol Cell Physiol*. 2002; 283(3):C905–C916.
16. Peti-Peterdi J, Sipos A. A high-powered view of

the filtration barrier. *J Am Soc Nephrol*. 2010; 21(11):1835–1841.
17. Devi S, et al. Multiphoton imaging reveals a new leukocyte recruitment paradigm in the glomerulus. *Nat Med*. 2013;19(1):107–112.
18. Schiessl IM, Bardehle S, Castrop H. Superficial nephrons in BALB/c and C57BL/6 mice facilitate in vivo multiphoton microscopy of the kidney. *PloS One*. 2013;8(1):e52499.
19. Hackl MJ, et al. Tracking the fate of glomerular epithelial cells in vivo using serial multiphoton imaging in new mouse models with fluorescent lineage tags. *Nat Med*. 2013;19(12):1661–1666.
20. Moeller MJ, Sanden SK, Soofi A, Wiggins RC, Holzman LB. Podocyte-specific expression of cre recombinase in transgenic mice. *Genesis*. 2003;35(1):39–42.
21. Chen Q, et al. Imaging neural activity using Thy1-GCaMP transgenic mice. *Neuron*. 2012; 76(2):297–308.
22. Zariwala HA, et al. A Cre-dependent GCaMP3 reporter mouse for neuronal imaging in vivo. *J Neurosci*. 2012;32(9):3131–3141.
23. Pippin JW, et al. Inducible rodent models of acquired podocyte diseases. *Am J Physiol Renal Physiol*. 2009;296(2):F213–F229.
24. Pippin JW, et al. Cells of renin lineage are progenitors of podocytes and parietal epithelial cells in experimental glomerular disease. *Am J Pathol*. 2013; 183(2):542–557.
25. Nakano D, et al. Multiphoton Imaging of the Glomerular Permeability of Angiotensinogen. *J Am Soc Nephrol*. 2012;23(11):1847–1856.
26. Salmon AHJ, et al. Loss of the endothelial glycocalyx links albuminuria and vascular dysfunction. *J Am Soc Nephrol*. 2012;23(8):1339–1350.
27. Peti-Peterdi J. Calcium wave of tubuloglomerular feedback. *Am J Physiol Renal Physiol*. 2006; 291(2):F473–F480.
28. Fischer KG, et al. Characterization of a Na+–Ca2+ exchanger in podocytes. *Nephrol Dial Transplant*. 2002;17(10):1742–1750.
29. McKanna JA, Chuncharunee A, Munger KA, Breyer JA, Cohen S, Harris RC. Localization of p35 (annexin I, lipocortin I) in normal adult rat kidney and during recovery from ischemia. *J Cell Physiol*. 1992; 153(3):467–476.
30. Dryer SE, Reiser J. TRPC6 channels and their binding partners in podocytes: role in glomerular filtration and pathophysiology. *Am J Physiol Renal Physiol*. 2010;299(4):F689–F701.
31. Fischer K-G, Saueressig U, Jacobshagen C, Wichelmann A, Pavenstädt H. Extracellular nucleotides regulate cellular functions of podocytes in culture. *Am J Physiol Renal Physiol*. 2001;281(6):F1075–F1081.
32. Bailey MA, et al. P2Y receptors present in the native and isolated rat glomerulus. *Nephron Physiol*. 2004; 96(3):p79–p90.
33. Ilatovskaya DV, Palygin O, Levchenko V, Staruschenko A. Pharmacological characterization of the P2 receptors profile in the podocytes of the freshly isolated rat glomeruli. *Am J Physiol Cell Physiol*. 2013;305(10):C1050–C1059.
34. Grgic I, Brooks CR, Hofmeister AF, Bijol V, Bonventre JV, Humphreys BD. Imaging of podocyte foot processes by fluorescence microscopy. *J Am Soc Nephrol*. 2012;23(5):785–791.
35. Höhne M, et al. Light microscopic visualization of podocyte ultrastructure demonstrates oscillating glomerular contractions. *Am J Pathol*. 2013; 182(2):332–338.
36. Matsusaka T, et al. Podocyte injury damages other podocytes. *J Am Soc Nephrol*. 2011;22(7):1275–1285.
37. Yaoita E, et al. Up-regulation of connexin43 in glomerular podocytes in response to injury. *Am J Pathol*. 2002;161(5):1597–1606.
38. Toma I, Bansal E, Meer EJ, Kang JJ, Vargas SL, Peti-Peterdi J. Connexin 40 and ATP-dependent intercellular calcium wave in renal glomerular endothelial cells. *Am J Physiol Regul Integr Comp Physiol*. 2008;294(6):R1769–R1776.
39. Isakson BE, Ramos SI, Duling BR. Ca2+ and inositol 1,4,5-trisphosphate-mediated signaling across the myoendothelial junction. *Circ Res*. 2007; 100(2):246–254.
40. Akerboom J, et al. Optimization of a GCaMP Calcium Indicator for Neural Activity Imaging. *J Neurosci*. 2012;32(40):13819–13840.
41. Chen TW, et al. Ultrasensitive fluorescent proteins for imaging neuronal activity. *Nature*. 2013; 499(7458):295–300.
42. Chevalier RL, Forbes MS, Thornhill BA. Ureteral obstruction as a model of renal interstitial fibrosis and obstructive nephropathy. *Kidney Int*. 2009; 75(11):1145–1152.
43. Forbes MS, Thornhill BA, Chevalier RL. Proximal tubular injury and rapid formation of atubular glomeruli in mice with unilateral ureteral obstruction: a new look at an old model. *Am J Physiol Renal Physiol*. 2011;301(1):F110–F117.
44. Schnermann J. Maintained tubuloglomerular feedback responses during acute inhibition of P2 purinergic receptors in mice. *Am J Physiol Renal Physiol*. 2011;300(2):F339–F344.
45. Schiessl IM, Castrop H. Angiotensin II AT2 receptor activation attenuates AT1 receptor-induced increases in the glomerular filtration of albumin: a multiphoton microscopy study. *Am J Physiol Renal Physiol*. 2013;305(8):F1189–F1200.
46. Sipos A, Vargas S, Peti-Peterdi J. Direct demonstration of tubular fluid flow sensing by macula densa cells. *Am J Physiol Renal Physiol*. 2010;299(5):F1087–F1093.